 doi:10.20944/preprints202205.0076.v1

Performance improvement of PCDTBT: $PC_{70}BM$ polymer solar cells with 1,8-diiodooctane solvent additive

Wenjuan Yu[1,*], Jiale Yang[1], Bingting Wang[1], Xiang Fu[1], Changhai Zhou[1], Haijun Zhou[1], Guoxiong Xie[1], Kexiu Dong[1] and Gan Jin[2]

[1]*School of Mechanical and Electronic Engineering, Chuzhou University, Chuzhou, 239000, People's Republic of China;*
[2]*School of Material Science and Chemical Engineering, Chuzhou University, Chuzhou, 239000, People's Republic of China.*
** Correspondence: yuwenjuan@chzu.edu.cn*

Abstract: The power conversion efficiency (PCE) of polymer solar cells (PSCs) are strongly depended on the bulk-heterojunction active layer. Here, the 1,8-diiodooctane (DIO) additives have been added into the PCDTBT: $PC_{70}BM$ blend PSCs. Based on the higher boiling point than host solvent ODB and better solubility of $PC_{71}BM$, the device photovoltaic properties with DIO additive were changed obviously. The investigations of EQE indicate that the DIO can influence the charge recombination and transportation process, and absorption studies demonstrate that the charge carriers generation process can also be affected by DIO. The overall impact reflected on the decreased equivalent resistant. With 3% v/v DIO, the J_{sc}, V_{oc} and FF are both increased. Correspondingly, a highest PCE is achieved of 6.15%, while the reference device without DIO only has a PCE of 5.23%. Hence, adding DIO solvent additive is a effective method for the photovoltaic properties improving of PCDTBT: $PC_{70}BM$ blend PSCs.

Keywords: polymer solar cells; solvent additive; DIO; PCDTBT

1. Introduction

Polymer solar cells (PSCs) have attracted more attentions in recent years due to the advantages of low-cost, light weight and facile fabrication process [1-3]. To realize high power conversion efficiency (PCE), bulk heterojunction (BHJ) structure active layer have been introduced with blending conjugated polymer as donor and fullerene derivative as acceptor [4]. Recently, the highest PCE of BHJ PSCs using low bandgap polymer have exceeded 18% [5]. For BHJ structure, the active layer morphology is the essential factor to achieve high PCE, because the interpenetrating network interfaces of phase separated donor and acceptor can affect the exciton separation and charge transportation [6]. If the phase separation process of active layer is incomplete, the exciton separation will be decline with misty interface. Meanwhile, if it is too complete, the charge trap will be developed with long transport distance. Hence, plenty strategies have been developed to modify the active layer morphology, such as material weight ratio treatment [7], thermal annealing [8, 9]

 doi:10.20944/preprints202205.0076.v1

and solvent engineering [10, 11]. In fact, the solvent plays important role which can influence the phase separation process with different solubility and boiling point. Consequently, the solvent engineering is a feasible way for morphology control which including solvent annealing [12], solvent mixed [13] and solvent additives [14-16].

Among these method, solvent additives has been proved to be an effective strategy for morphology control. Here, the active layer is a mixture with four element: polymer donor, fullerene acceptor, host solvent and extra additive. The utilization of additive into primary host solvent is one of the simplest and convenient method for solvent management because there is no other additional fabrication process [17]. As we known, during solvent evaporation, the interpenetrating network structure with polymer and fullerene domains will be fabricated from liquid to liquid phase separation process. Hence, there are two criteria for additives selection, including greater boiling point than host solvent and different solubility for polymer and fullerene. The different boiling point of two solvent will influence the evaporation speed. Furthermore, the different domains size of polymer and fullerene will be developed during materials integration process under variable solvent evaporation speed. Consequently, through combining the additives into solvent, the morphology of BHJ active layer can be changed which can effect the device performance.

Some additives with high boiling point have been used to modify the morphology of active layer in PSCs, such as 1-chloronaphthalene (CN) [18], 1,8-octanedithiol (OT) [19], N-methyl pyrrolidone (NMP) [20] and 1,8-diiodooctane (DIO) [21-23]. For example, Lee *et al.* reported that DIO is a effective additives by adding various 1,8-di(R)octanes classes with different R-groups into PSCs [21]. Liang *et al.* stated that the morphology of PTB7: $PC_{71}BM$ in chlorobenzene with DIO additive has much more smaller phase separation [22]. Lou *et al.* explained that smaller phase separation means smaller domains of polymer and fullerene, and superior interpenetrating network can be induced by DIO additive [23]. Additionally, DIO can also affect the carrier transportation and recombination, suggesting that the DIO may influence the photovoltaic performance by adjusting the volume ratio. Subsequently, in this work, DIO has been added into o-dichlorobenzene host solution based on poly[N-9''-hepta-decanyl-2,
7-carbazole-alt-5,5-(4',7'-di-2-thienyl-2',1',3'-benzothiadiazole)
(PCDTBT): [6, 6]-phenyl C_{71}-butyric acid methyl ester ($PC_{71}BM$) blend [24]. The results indicated that the PCE is increased from 5.23% to 6.15% with distinct Jsc, Voc and FF with 3% volume ratio of DIO. We have investigated the PSC photovoltaic characterization, absorption and complex impedance analysis with different volume ratio of DIO. Our experimental reveals that the DIO additive not only affect the absorption, but also influence the series resistance. This work demonstrated that the photovoltaic improvement will be obtained in PSCs processed with DIO additive.

 doi:10.20944/preprints202205.0076.v1

2. Materials and Methods

2.1. Preparation of Titanium Dioxide Precursor

Sol-sel Titanium Dioxide (TiO_2) precursor [25, 26] were prepared from tetrabutyl titanate ($Ti(OC_4H_9)_4$). Firstly, 10ml ($Ti(OC_4H_9)_4$) and 5ml acetyl acetone were dissolved into 90ml ethanol (C_2H_5OH). Then, 10ml CH_3COOH and 10ml de-ionized water were added into the solution under vigorous stirring in 2h.

2.2. PSC Devices Fabrication

The device structure is ITO /TiO_2 /PCDTBT: $PC_{71}BM$ /WO_3 /Ag, which is schematically shown in Fig. 1(a). The substrate is used the patterned ITO-coated glass with sheet resistance of 15Ω/sq. Firstly, the ITO was cleaned by acetone, ethanol and de-ionized water for 30 minutes respectively and then treated by UV-Ozone for 20min to increase the hydrophilia and work function. Subsequently, the sol-sel titanium dioxide (TiO_2) precursor was cast onto ITO substrate at 3000rpm by spin coating. The samples were annealed 2h at 450℃ in the muffle furnace, leading to an anatase polycrystalline oxide film of TiO_2. Then, 7mg PCDTBT (Lumtec Corp) and 28mg $PC_{71}BM$ (Lumtec Corp) (1:4 weight ratio) were dissolved into 1ml o-dichlorobenzene (ODB) at room temperature with a concentration of 7 mg/ml. The DIO additive was added into host solvent ODB with 3% and 5% (volume ratio v/v). The PCDTBT: $PC_{71}BM$ film was spin coated onto TiO_2 film at 1000rpm and thermally annealed at 70℃ for 25min in the glove box. Finally, the 10nm WO_3 and 80nm Ag were vacuum evaporated in sequence under 5×10^{-4} Pa condition without disrupting the vacuum. In order to define the area of PSC device, the Ag top electrode was evaporated through a shadow mask. The area is about 0.064 cm^2 and the dimension is 0.32cm*0.2cm. The deposition rate was about 0.3 nm/s, which was monitored by a quartz-oscillating thickness monitor (ULVAC, CRTM-9000).

The current density-voltage (J–V) characteristics were measured by the computer-programmed Keithley 2601 source meter under an irradiation intensity of AM 1.5G by an Oriel 300 W solar simulator intensity of 100 mW/cm^2 (about one sun). The light intensity was measured by a photometer (International light, IL1400) corrected by a standard silicon solar cell. The absorption spectrum was measured by an ultraviolet/visible spectrometer (UV3600, Shimadzu). IPCE spectra were measured by Crowntech QTest Station 1000AD. Impedance spectroscopy were measured with an AC signal of 1 V by an impedance analyzer (Wayne Kerr Electronics 6520B) in the frequency from 20 Hz to 2 MHz. All the tests were measured in the air without encapsulation at room temperature.

3. Results

The device schematic diagram and the chemical structures of used materials PCDTBT, $PC_{71}BM$ and DIO are shown in Fig. 1. In the device structure, the transparent ITO electrode is used as the cathode and the opaque Ag electrode is used as the anode.

 doi:10.20944/preprints202205.0076.v1

The bulk-heterojunction of PCDTBT and $PC_{71}BM$ has an interpenetrating network structure after solvent annealing. The energy level diagram is shown in Fig. 2. The highest occupied molecular orbital (HOMO) level and the of lowest unoccupied molecular orbital (LUMO) level of PCDTBT and $PC_{71}BM$ are -5.5 eV, -3.6 eV and -6.0 eV, -4.1 eV respectively [27]. TiO_2 film [28] with a very low HOMO level (-8.0 eV) is act a electron transportation layer, which can prevent the holes transportation effectively and transport the electron carriers at the same time. WO_3 is a common used hole transport layer which can transport the hole carriers and prevent the electron transportation [29]. As known, the exciton separated into free electron and hole carriers at the interfaces of interpenetrating network of PCDTBT and $PC_{71}BM$. Within the carriers transportation process from active layer to electrode collection, the recombination can take place at anywhere. Accordingly, due to the ability of carrier filtrate of TiO_2 and WO_3 layers in the device, the carriers recombination can be avoided in the transportation process beside the active layer to the electrode. Here, we introduce the DIO solvent additive into ODB host solvent in the PCDTBT: $PC_{71}BM$ mixture. The DIO not only has higher boiling point than ODB, but also has better solubility of $PC_{71}BM$. By influencing the interfaces of PCDTBT and $PC_{71}BM$, the carriers recombination can be changed in the transportation process inside the active layer.

In order to optimize the DIO volume ratio, 3% and 5% v/v volume ratio have been added into ODB. Fig. 3a shows photo current density-voltage J-V characteristics of PSCs with different volume ratio DIO additive under illumination of AM 1.5G, 100 mW/cm^2. As observed, the J-V parameters are changed obviously with DIO additive. The reference device without any additive shows a short circuit current density (J_{sc}) of 11.23 mA/cm^2, a open circuit voltage (V_{oc}) of 0.85V, a fill factor (FF) of 54.8%, and indeed PCE of 5.23%. With 3% v/v DIO, the J_{sc}, V_{oc}, FF are both increased to 11.96 mA/cm^2, 0.87 V, and 59.1% respectively. As a result, a highest PCE of 6.15% is expected. Then, with higher 5% v/v DIO, the J_{sc}, V_{oc}, FF are both dropped to 10.33 mA/cm^2, 0.81V, and 47.9% respectively. Correspondingly, the lowest PCE is 4.01%. The detail data of J_{sc}, V_{oc}, FF, PCE, series resistance R_s and shunt resistance R_{sh} are listed in Table I. Compared to the reference device without DIO, the devices processed with DIO additives have a distinct photovoltaic parameter. For 3% v/v DIO, there is a positive effect, but for 5% v/v DIO, the effect is negative.

In order to understand the heterojunction photovoltaic conversion property, the dark current curves under single logarithmic have been tested as shown in Fig. 4a. For device with 3% v/v DIO, the leakage current is the smallest and the turn-on current is largest. As is well known, the leakage current is influenced by the shunt resistance R_{sh}, which represents the charge carrier recombination. Meanwhile, the turn-on current is determined by series resistance (R_s) that indicates the heterojunction semiconductor bulk resistance and means the charge transportation furthermore. For device with 3% v/v DIO, the smallest leakage current represents the decreased charge

 doi:10.20944/preprints202205.0076.v1

carrier recombination in active layer and the largest turn-on current means the superior transportation and well ETL/active layer/HTL interfaces. At the same time in the dark current curves, the break point of reference device with 3% v/v DIO additive is larger than that of device without DIO. Correspondingly, the break point is relate to the Voc [30]. For device with 3% v/v DIO additive, the break point is the most on the right with voltage bias, which results a relative highest Voc under AM 1.5G illumination.

The relationship between photo current density (J_{ph}) curves and the effective applied bias V_{eff} is shown in Fig 4b. Here, J_{ph} is regarded as the difference between the current density J_{light} under AM 1.5G illumination and the current density J_{dark} under dark condition, and thus $J_{ph} = J_{light} - J_{dark}$. The V_{eff} is termed as the difference between the voltage bias V_0 while the J_{ph} equals to zero and voltage bias V, and so $V_{eff}=V_0 - V$. As we can see, under lower effective applied bias V_{eff} (< 0.2V), the J_{ph} changed smoothly and linearly. With higher V_{eff} (> 0.2V), the increment rate decreased gradually. When V_{eff} > 10V, the J_{ph} was in the saturation state for both devices with or without DIO while the J_{ph} is defined as J_{sat}. For reference device without DIO, the J_{sat} is 10.77 mA/cm^2, but it is 11.79 mA/cm^2 for device with 3% v/v DIO. The increased J_{sat} was attributed to the decreased Rs by the DIO additive induced superior heterojunction interpenetrating network with decreased recombination and increased transportation. At the same time, the J_{ph} of device without DIO was the first one coming into the saturation state while V_{eff} > 0.2V. This phenomenon indicates that with DIO, the device is less likely to saturate, which provides a space for photo current enhancement.

In order to detailed investigate the growth of photo current J_{sc}, the EQE has been analyzed in Fig. 5. As known, there is a relationship between EQE and the J_{sc} as follows [31, 32].

$$J_{sc} = \int \frac{q\lambda}{hc} EQE(\lambda) S(\lambda) d\lambda \quad (1)$$

Where the S(λ) is the spectral density of AM 1.5G illumination under 100 mW/cm^2 . As in Fig. 5, a increased EQE is achieved in device with 3% v/v DIO, especially in wavelength range from 380 nm to 700 nm. The maximum EQE is about 58.5% at 540 nm. Based on the Equation (1), the enhancement of EQE is corresponding to the increased J_{sc}. The shapes of EQE curves are all the same, indicating that there is no additional absorption. The EQE is regarded as the ratio of number of the collected charge carriers by the electrode to number of the illuminated photons by the illumination. It includes the recombination and the transportation process in the device, but cannot demonstrate the IQE conversion process, which means the ratio of the number of collected charge carriers by the electrode to number of absorbed photons by the active layer. Here, the IQE is related to the EQE and absorption as follows [33].

$$IQE(\lambda) = EQE(\lambda)/Abs(\lambda) \quad (2)$$

Where the Abs(λ) is represent the absorption of the device. Hence, the absorption spectra are tested and shown in Fig. 6. The

 doi:10.20944/preprints202205.0076.v1

shapes of the spectra are also not changed obviously fitting to the EQE spectra shapes. There is a slight decrease for the device with 3% v/v DIO than that of the device without DIO. Conversly, the EQE has a increasement for the device with 3% v/v DIO. According to the Equation (2), a significant increased IQE can be expected for the device with 3% v/v DIO. It is indicates that with DIO, more photons are separated into the electron and hole charge carrier pairs. Consequently, the separation process is optimized by the DIO additives.

Hence, the DIO can influence the separation, recombination and the transportation process of the PSC. The feasibility collected charge carriers property can also manifest as the resistance performance in the macroscopic device. In order to show the influence of interface resistance, the complex impedance spectra of the devices with or without DIO were measured in dark condition [34]. With the test frequency ranging from 20 Hz to 2 MHz, the impedance spectra are treated into Nyquist diagrams that the real part (ReZ) of the complex impedance is the product of complex impedance of cosine of the phase and the imaginary part (ImZ) of the complex impedance is the product of complex impedance of sine of the phase. According to the data treatment, two semicircles' shapes are formed in the first quadrant in Nyquist diagrams. As shown in the right corner of Fig. 7, the inset model is the equivalent R-C circuit of PSC, which includes a equivalent resistant and a equivalent capacitance in parallel. Here, the diameter of semicircle can represent the equivalent resistant of PSC. It is obvious that the two diameter are distinct, while semicircle of the device with 3% v/v DIO is much smaller. It is means smaller equivalent resistant in the device. The result is corresponding to the decreased Rs in the J-V characteristics. It is demonstrated that with 3% v/v DIO, the interface transportation and electrode collection process can be optimized and a increased PCE can be obtained.

4. Conclusions

In conclusion, the PSC devices with and without DIO solvent additive were investigated based on PCDTBT: $PC_{70}BM$ bulk - heterojunction active layer. With 3% v/v DIO, the J_{sc}, V_{oc} and FF are both increased. Hence, a highest PCE is achieved at 6.15%, while the reference device without DIO only has a PCE of 5.23%. The EQE spectra were studied and the results show that the DIO can influence the transportation process. The increased IQE based on increased EQE and slightly decreased absorption means the DIO can also influence the exciton separation process. Hence, the feasibility collection process can exhibit a lower equivalent resistant corresponding to the series resistant. The investigation of DIO solvent additives shows that the DIO is a effective solvent for PCDTBT: $PC_{70}BM$ PSCs. Furthermore, this work provide a useful and a simple guideline for the additive selection method to increase the PCE of PSC.

Author Contributions: Conceptualization, Wenjuan Yu and Jiale Yang; software, Bingting Wang; validation, Gan Jin; formal analysis, Xiang Fu;

investigation, Guoxiong Xie; resources, Changhai Zhou; data curation, Haijun Zhou; writing—original draft preparation, Wenjuan Yu; writing—review and editing, Wenjuan Yu; funding acquisition, Kexiu Dong. All authors have read and agreed to the published version of the manuscript.

Funding: This research was funded by the National Natural Science Foundation of China (No. 22109017), the Natural Science Foundation of the Anhui Higher Education Institutions (No. KJ2020A0710, No. KJ2021B11), and the Scientific Foundation of Chuzhou University (No. 2022qd035).

References

[1] J.Y. Kim, K. Lee, N.E. Coates, D. Moses, T.Q. Nguyen, M. Dante, A.J. Heeger, Efficient Tandem Polymer Solar Cells Fabricated by All-Solution Processing, *Science* **2007**, *317,* 222-225.

[2] F. Kaka, M. Keshav, P.C. Ramamurthy, Optimising the photovoltaic parameters in donor–acceptor–acceptor ternary polymer solar cells using Machine Learning framework, *Solar Energy* **2022**, *231*, 447-457.

[3] Y. Ma, D. Cai, S. Wan, P. Yin, Q. Zheng, Control over π-π stacking of heteroheptacene-based nonfullerene acceptors for 16% efficiency polymer solar cells, *National Science Review* **2020**, *7*, 12.

[4] G. Yu, J. Gao, J. C. Hummelen, F. Wudl, A. J. Heeger, Polymer photovoltaic cells: enhanced efficiencies via a network of internal donor-acceptor heterojunctions, *Science* **1995**, *270*, 1789.

[5] M. Zhang, L. Zhu, G. Zhou, T. Hao, F. Liu, Single-layered organic photovoltaics with double cascading charge transport pathways: 18% efficiencies, *Nature Communication* **2021,** *12*, 309.

[6] Z. He, C. Zhong, S. Su, M. Xu, H. Wu, Y. Cao, Enhanced power-conversion efficiency in polymer solar cells using an inverted device structure, *Nature Photonics* **2012**, *6*, 591–595.

[7] J. Yuan, H. Dong, M. Li, X. Huang, J. Zhong, Y. Li, W. Ma, High Polymer/Fullerene Ratio Realized in Efficient Polymer Solar Cells by Tailoring of the Polymer Side-Chains, A*dvanced Materials* **2014**, *26*, 3624-3630.

[8] Y.Y. Lee, K.H. Tu, C.C. Yu, S.S. Li, J.Y. Hwang, C.C. Lin, K.H. Chen, L.C. Chen, H.L. Chen, C.W. Chen, Top laminated graphene electrode in a semitransparent polymer solar cell by simultaneous thermal annealing/releasing method, *Acs Nano* **2011**, *5*, 6564-6570.

[9] Z. Lin, L. Zhang, S. Tu, W. Wang, Q. Ling, Highly thermally stable all-polymer solar cells enabled by photo-crosslinkable bromine-functionalized polymer donors, *Solar Energy* **2020**, *201*, 489-498.

[10] D. Khatiwada, S. Venkatesan, J. Chen, Q. Chen, N. Adhikari, A. Dubey, A.F. Mitul, L. Mohammad, J. Sun, C. Zhang, Morphological Evolution and Its Impacts on Performance of Polymer Solar Cells, *IEEE Transactions on Electron Devices* **2015**, *62*, 1284-1290.

[11] X. Guo, M. Zhang, W. Ma, S. Zhang, J. Hou, Y. Li, Effect of solvent additive on active layer morphologies and photovoltaic performance of polymer solar cells based on PBDTTT-C-T/PC71BM, *Rsc Advances* **2016**, *6*, 51924-51931.

[12] L. Chang, H. W. A. Lademann, J. B. Bonekamp, K. Meerholz and A. J. Moule, Effect of Trace Solvent on the Morphology of P3HT:PCBM Bulk Heterojunction Solar Cells, *Advanced Functional Materials* **2011**, *21*, 1779-1787.

[13] S. Lee, D. Jeong, C. Kim, C. Lee, B.J. Kim, Eco-Friendly Polymer Solar Cells: Advances in Green-Solvent Processing and Material Design, *Acs Nano* **2020**, *14*, 14493-14527.

[14] J.J. Van Franeker, M. Turbiez, W. Li, M.M. Wienk, R.A.J. Janssen, A real-time study of the benefits of co-solvents in polymer solar cell processing, *Nature Communications* **2015**, *6*, 6229.

[15] M. Shang, X. Yu, Y. Xu, H. Wang, L. Hui, Effect of different solvents on the performance of ternary polymer solar cells based on PTB7:PC71BM:F8BT, *Journal of Physics D: Applied Physics* **2015**, *48*, 295105.

[16] T. Dai, X. Li, Y. Zhang, D. Xu, X. Chen, Performance improvement of polymer solar cells with binary additives induced morphology optimization and interface modification simultaneously, *Solar Energy* **2020,** *201*, 330-338.

[17] Y. Zheng, S. Li, Z. Ding, J. Yu, Effects of different polar solvents for solvent vapor annealing treatment on the performance of polymer solar cells, *Organic Electronics* **2014**, *15*, 2647-2653.

[18] M. Li, L. Wang, J. Liu, K. Zhou, X. Yu, R. Xing, Y. Geng, Y. Han, Cooperative effects of solvent and polymer acceptor co-additives in P3HT:PDI solar cells: simultaneous optimization in lateral and vertical phase separation, *Physical Chemistry Chemical Physics* **2014**, *16*, 4528-4537.

[19] H.Y. Chen, H. Yang, G. Yang, S. Sista, R. Zadoyan, G. Li, Y. Yang, Fast-Grown Interpenetrating Network in Poly(3-hexylthiophene): Methanofullerenes Solar Cells Processed with Additive, The *Journal of Physical Chemistry C* **2009**, *113*, 7946-7953.

[20] H. Jung, A.R. Jung, S.M. Jin, S. Kim, B.S. Kim, Influence of 3D morphology on the performance of all-polymer solar cells processed using environmentally benign nonhalogenated solvents, *Nano Energy* **2020**, *77*, 105106.

[21] J.K. Lee, W.L. Ma, C.J. Brabec, J. Yuen, J.S. Moon, J.Y. Kim, K. Lee, G.C. Bazan, A.J. Heeger, Processing additives for improved efficiency from bulk heterojunction solar cells, *Journal of the American Chemical Society* **2008**, *130*, 3619-3623.

[22] Y. Liang, R. Xu, R. Xia, R.T. Tsai, R. Wu, R. Li, C. Ray, R. Yu, For the Bright Future-Bulk Heterojunction Polymer Solar Cells with Power Conversion Efficiency of 7.4%, *Advanced Materials* **2010**, *22*, P.E135-E138, E195.

[23] S.J. Lou, J.M. Szarko, T. Xu, L. Yu, T.J. Marks, L.X. Chen, Effects of additives on the morphology of solution phase aggregates formed by active layer components of high-efficiency organic solar cells, *Journal of the American Chemical Society* **2011**, *133*, 20661-20663.

[24] L. Jian, S. Shao, F. Gang, B. Meng, Z. Xie, L. Wang, High-Efficiency Inverted Polymer Solar Cells with Transparent and Work-Function Tunable MoO3-Al Composite Film as Cathode Buffer Layer, *Advanced Materials* **2012**, *24*, 2774-2779.

[25] T. Chen, S. Ruan, X. Zhang, G. Xie, S. Liang, X. Kong, D. Wei, C. Liu, W. Chen, Performance improvement of inverted polymer solar cells with different top electrodes by introducing a MoO3 buffer layer, *Applied Physics Letters* **2008**, *93*, 411.

[26] Hailin, Xue, Xiangzi, Kong, Ziran, Liu, Caixia, Jingran, Zhou, TiO2 based metal-semiconductor-metal ultraviolet photodetectors, *Applied Physics Letters* **2007**, *90*, 223505.

[27] N. Blouin, A. Michaud, M. Leclerc, A Low-Bandgap Poly(2,7-Carbazole) Derivative for Use in High-Performance Solar Cells, *Advanced Materials* **2007**, *19*, 2295-2300.

[28] H.L. Yip, K.Y. Jen, Recent advances in solution-processed interfacial materials for efficient and stable polymer solar cells, *Energy & Environmental Science* **2012**, *5*, 5994-6011.

[29] T. Chen, S. Ruan, G. Xie, X. Kong, S. Liang, F. Meng, C. Liu, X. Zhang, W. Dong, W. Chen, Role of tungsten oxide in inverted polymer solar cells, *Applied Physics Letters* **2009**, *94*, 29.

[30] Z. Ling, S. Zhao, X. Zheng, Q. Bo, H. Di, X. Xu, Two effects of 1,8-diiodooctane on PTB7-Th:PC71BM polymer solar cells, *Organic Electronics* **2016**, *34*, 188-192.

[31] Letian, Dou, Jingbi, You, Ziruo, Hong, Zheng, Xu, Gang, Li, 25th Anniversary Article: A Decade of Organic/Polymeric Photovoltaic Research, *Advanced Materials* **2013**, *25*, 6642–71.

 doi:10.20944/preprints202205.0076.v1

[32] H. Wang, Y. Zheng, L. Zhang, J. Yu, Effect of two-step annealing on the performance of ternary polymer solar cells based on P3HT:PC71BM:SQ, *Solar Energy Materials & Solar Cells* **2014,** *128*, 215-220.

[33] G. Dennler, K. Forberich, M.C. Scharber, C.J. Brabec, T. Fromherz, Angle dependence of external and internal quantum efficiencies in bulk-heterojunction organic solar cells, J*ournal of Applied Physics* **2007**, *102*, 1789.

[34] Z.A. Tan, C. Yang, E. Zhou, W. Xiang, Y. Li, Performance improvement of polymer solar cells by using a solution processible titanium chelate as cathode buffer layer, *Applied Physics Letters* **2007**, 91, 1324.

Table I The detail data of devices with or without DIO additive.

Deivice	V_{oc} (V)	J_{sc} (mA/cm^2)	*FF* (%)	PCE(%)	R_s(Ω·cm^2)	R_{sh}(Ω·cm^2)
Without DIO	0.85	11.23	54.8	5.23	15.4	3.5
3% v/v DIO	0.87	11.96	59.1	6.15	12.3	1.26
5% v/v DIO	0.81	10.33	47.9	4.01	16.5	0.58

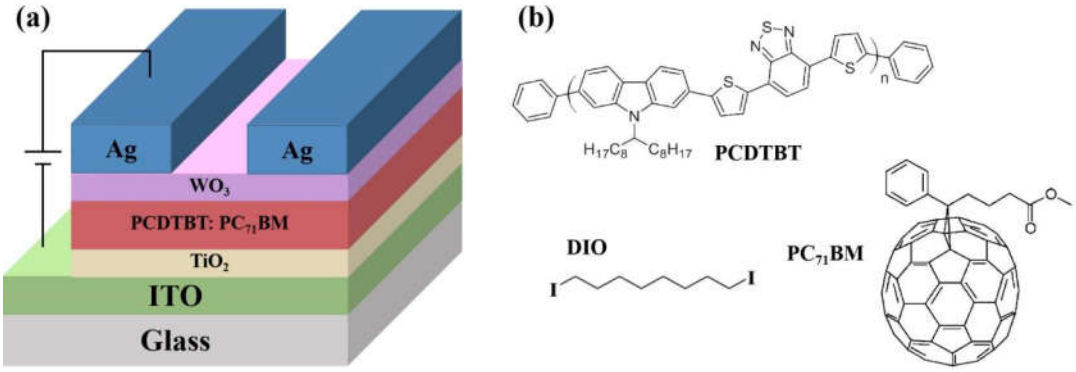

Fig. 1 (a) PSC device schematic structure; (b) Chemical structures of PCDTBT, $PC_{71}BM$ and DIO.

Preprints (www.preprints.org) | NOT PEER-REVIEWED | Posted: 6 May 2022 doi:10.20944/preprints202205.0076.v1

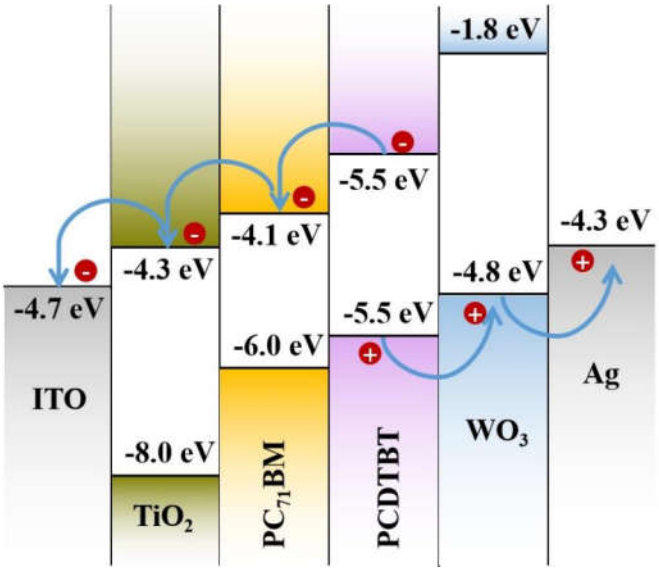

Fig. 2 Energy level of the PSC device.

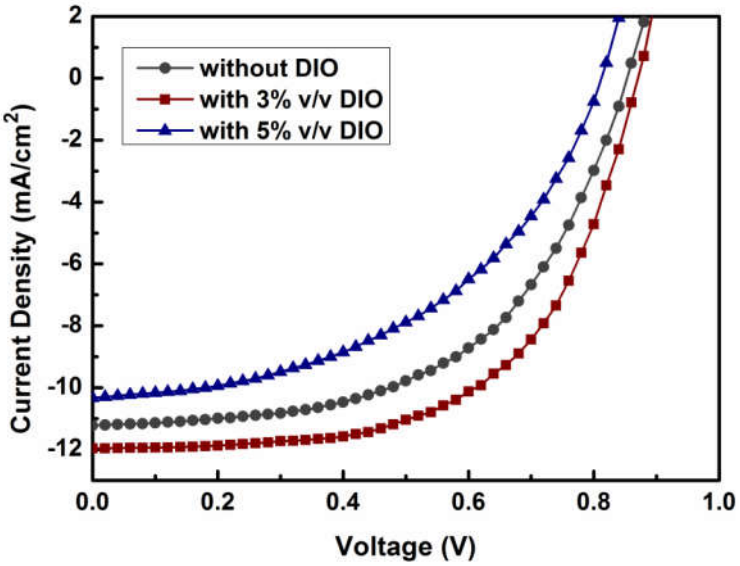

Fig. 3 Photo current J-V characteristics of PSCs with different volume ratio DIO additive under illumination of AM 1.5G, 100 mW/cm^2;

Preprints (www.preprints.org) | NOT PEER-REVIEWED | Posted: 6 May 2022 doi:10.20944/preprints202205.0076.v1

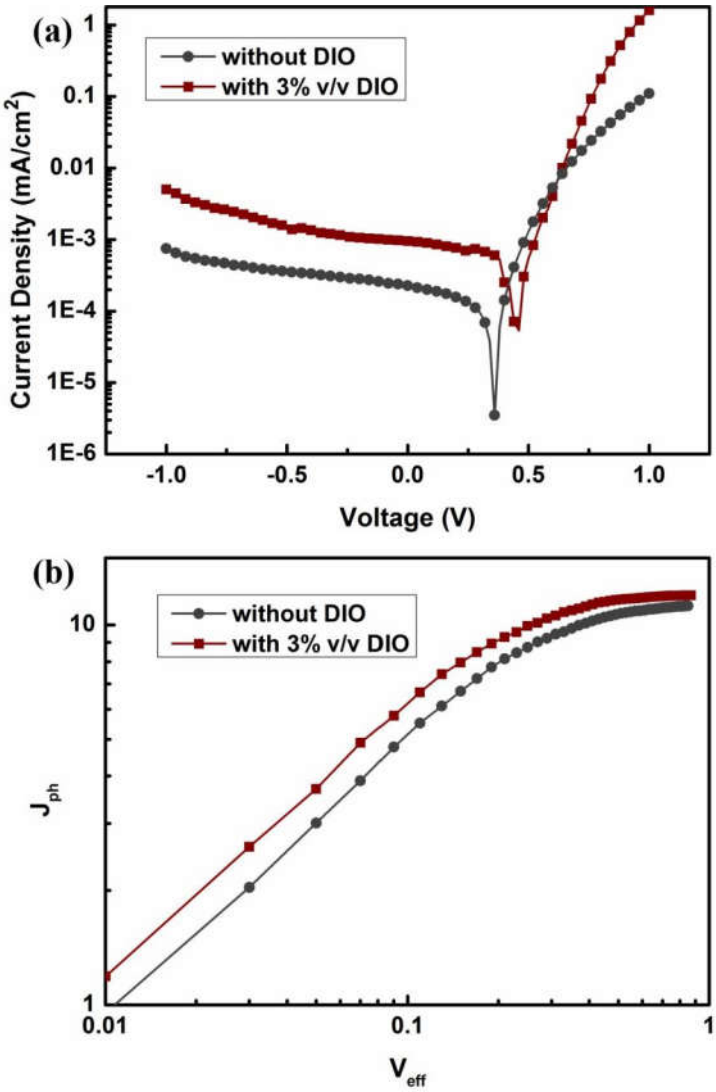

Fig. 4 (a) Single logarithmic dark current J-V curves of PSCs with different volume ratio DIO additive; (b)The function of photo current density (J_{ph}) curves with the effective applied bias V_{eff}.

Preprints (www.preprints.org) | NOT PEER-REVIEWED | Posted: 6 May 2022 doi:10.20944/preprints202205.0076.v1

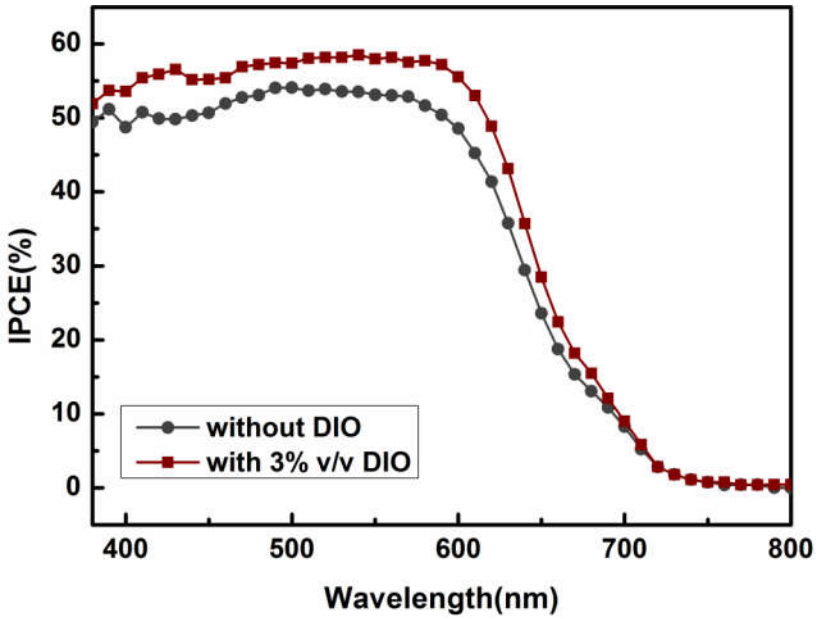

Fig. 5 The IPCE (EQE) curves of devices with or without DIO additive.

Preprints (www.preprints.org) | NOT PEER-REVIEWED | Posted: 6 May 2022 doi:10.20944/preprints202205.0076.v1

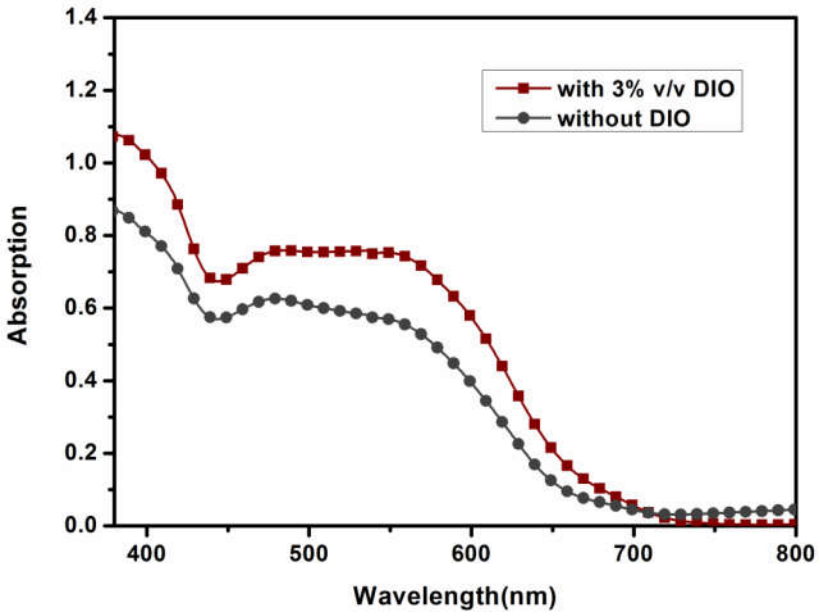

Fig. 6 The absorption spectra of PCDTBT: $PC_{71}BM$ with or without DIO additive.

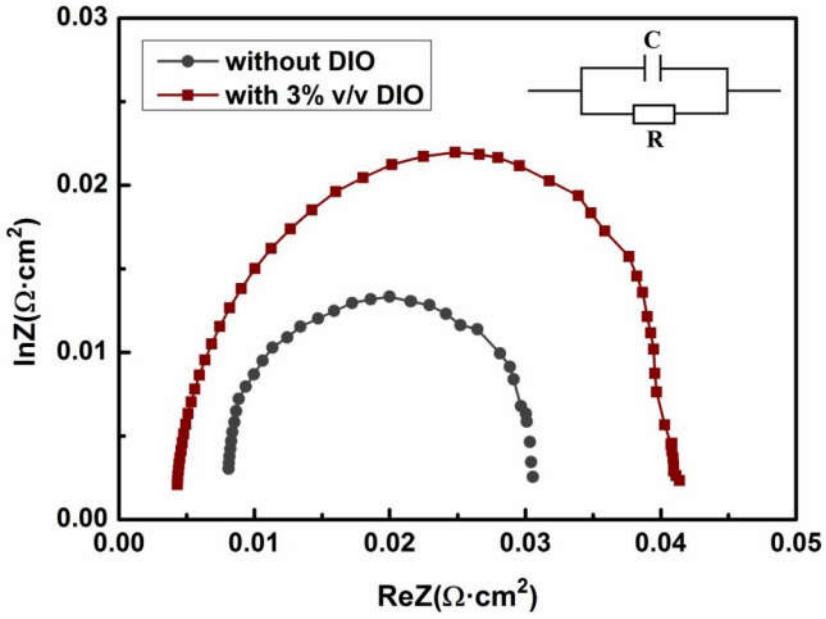

Fig. 7 The Nyquist diagrams of complex impedance spectra of the devices with or without DIO in dark condition at 0 V. Inset: Equivalent R-C circuit model of PSC.